ChemComm

Formation of Nanostructured Silicas through the Fluoride Catalysed Self-Polymerization of Q-type Silsesquioxane Cages

Journal:	*ChemComm*
Manuscript ID	CC-COM-05-2022-002672.R1
Article Type:	Communication

COMMUNICATION

Formation of Nanostructured Silicas through the Fluoride Catalysed Self-Polymerization of Q-type Functional Silica Cages

Received 00th January 20xx,
Accepted 00th January 20xx

DOI: 10.1039/x0xx00000x

Nai-hsuan Hu,[a] Cory B. Sims,[a] Tyler V. Schrand,[a] Kathryn M. Haver,[a] Herenia Espitia Armenta,[a] and Joseph C. Furgal*[a]

Octa(dimethylsiloxy)silica cages ($Q_8M_8^H$) undergo rapid self-polymerization in the presence of a fluoride catalyst to form complex 3D porous structural network materials with specific surface areas up to 650 m^2g^{-1}. This establishes a new method to bio-derived high inorganic content soft silicas with potential applications in filtration, carbon capture, catalysis, or hydrogen source.

Porous materials and methods to control their properties in a simple cost effective manner such as pore size, crystallinity, and functionality are highly sought after for applications ranging from substance capture to catalysis.[1,2] Silicon and its various forms of cubic structures offer exceptional ways to achieve these goals.[3] Many functional silicon-based porous materials have been synthesized to impart high porosity, specific surface areas (SSA), and functionalities often through sol-gel type chemistries with alkoxysilanes, or through network polymerization of cage-type molecules (polyhedral oligomeric silsesquioxanes, POSS)[4–6] or Q-type silica cages;[7–9] Liu et al.[3] and Shimojima et al.[7] have both published excellent recent reviews of these efforts. While these systems offer high SSA and functionalization potential, most of them still result in amorphous materials with relatively little structural control.

Herein we focus on the use of the Q-cage. The Q-type silica cages are an excellent building block for materials as a highly stable cubic form of silica that is derivable from the agricultural by-product rice hull ash.[10,11] These silica Q-cages are functionalissable with various R-chlorodimethylsilanes to impart groups reactable by hydrosilylation,[12] sol-gel,[10] thiol-ene,[13] or other methods.[10] Octa(dimethylsiloxy)cubic-silica ($Q_8M_8^H$, Si-H) is a workhorse form of Q-cage due to its ability to be functionalized through common hydrosilylation methods.

Q-cages have found use in porous and high surface area materials and show propensity toward crystalline and periodic geometries more structurally analogous to zeolites.[14] For example, Sato et. al. successfully demonstrated the first Q-cage-based crystalline network materials from $Q_8M_8^H$ by Pd/C catalysed hydrolysis to free silanols (-$SiMe_2OH$), followed by co-crystallisation with trimethylbenzene.[4] These cages were then locked into the network using chlorosilanes to obtain microporous materials with SSA up to 475 m^2g^{-1}. The remaining unhydrolyzed Si-H groups could be further functionalized to induce pore modification. Pan et. al. have used $B(C_6F_5)_3$ catalysed Piers-Rubinsztajn(oxysilylation) reactions to give 3D networks with periodicity and BET surface areas up to 700 m^2g^{-1} under mild conditions (hexane/60°C) and short reaction times of 20-40 minutes.[9] Both of these methods use rather expensive catalysts and more efficient methods are needed to develop new crystalline and amorphous Q-cage materials.

Our research group has developed highly porous POSS systems with cheap fluoride (F^-) catalysed sol-gel methods from R-alkoxysilanes.[15,16] In that work we found that solvent choice for the sol-gel chemistry could be used to vastly alter the porosity, surface areas, and textures of the synthesized networks. Inspired by that methodology and pure curiosity, we began exploring F^- interactions with Q-cages, finding rapid reactivity to form polymeric materials. In this work we use F^- to trigger the self-polymerization between $Q_8M_8^H$ cages to form nanostructured silicas and showcase initial work toward understanding the mechanistic processes taking place. A series of reaction conditions (i.e. solvents) were investigated and compared using spectroscopic methods. Various catalysts are investigated as well as comparisons to $Q_8M_8^{Me}$ (-O-$SiMe_3$). By these methods, functionalization can be performed before polymerization, which can largely decrease the challenges in making highly functional porous materials.

From our recent studies,[15,16] dichloromethane (DCM, $Q_8M_8^H$ soluble) and acetonitrile (ACN, $Q_8M_8^H$ ~insoluble) were the solvent systems preferred for network formation and are the model solvents here (**Scheme 1, Fig. S1, Table S1**), with toluene, acetone, methanol, and 1:1 DCM:ACN also explored. Note that CSF and tetramethylammonium hydroxide [TMAH] as catalysts

[a] *Department of Chemistry and Center for Photochemical Sciences Bowling Green State University, Bowling Green, OH 43403 USA.*

† Electronic Supplementary Information (ESI) available: Including experimental details and additional characterization data. See DOI: 10.1039/x0xx00000x

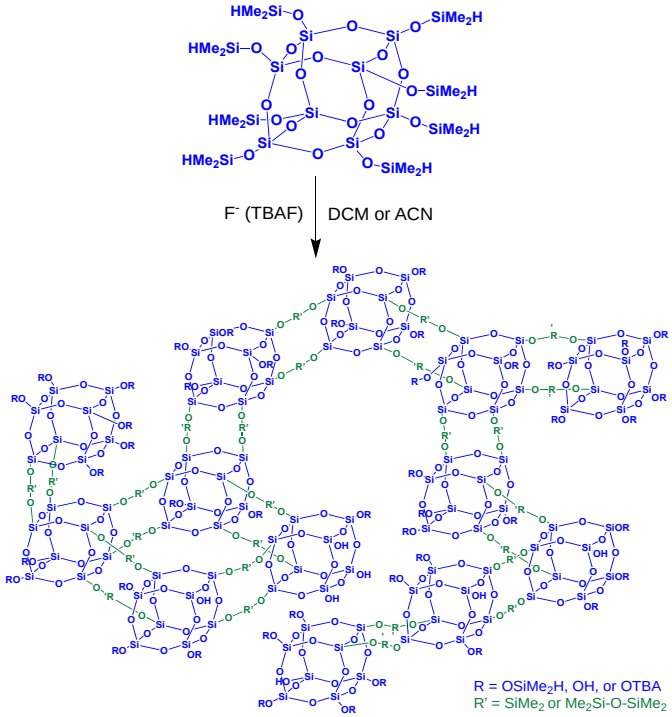

Scheme 1. Proposed self-linking polymerization of $Q_8H_8^H$ cages with TBAF catalysis.

and $Q_8M_8^{Me}$ as Q-cage were also explored with details given in **SI**. In the simple reaction, $Q_8M_8^H$ cage was added to solvent followed by 3 mol% tetra-n-butylammonium fluoride (TBAF, 1M in THF, ~5% H_2O) catalyst to initiate the reaction. We observed that reactions in all solvent systems evolved large amounts of gas. For insight into the gas and understanding the reaction process, we employed GC-MS through headspace analysis and a universal gas analyzer in-situ to identify H_2, $SiHMe_2OH$, and SiH_2Me_2 (**Fig. S2, S3**) as the evolved gases. Since F^- commonly show limited reactivity with silica (SiO_2), and the evolved gases are made up of components from the peripheral groups, we proposed that the polymerization happens through interactions between F^- and $-OSiMe_2H$ corners (**Scheme 2**), leaving the cage itself intact. From gas analysis results, we anticipated that the reaction must involve the release of H^- post pentacoordinated intermediate formation in a first step post F^- attack. These reactions are confirmed from the literature,[17–19] with F^- effectively displacing H^- from a pentacoordinate intermediate of trimethylsilane being known since at least 1973.[20] After F^- attacks, released H^- reacts with either a proton source (i.e. H_2O) to form $H_{2(g)}$ or substitutes another $-SiMe_2H$ group to remove $SiMe_2H_2$, with both methods forming oxygen nucleophiles. The new nucleophile can further react with $Q_8M_8^H$ to trigger cleavage of $-SiMe_2H$, initiating polymerization. Formed anions likely form salts with tetrabutylammonium ($TBAF_{cat}$).[21,22]

Reactions of $Q_8M_8^H$ in both DCM and ACN emit the same gases, however, significant differences in the reaction times and final network products are observed (**Fig. S1a**). The reaction in ACN occurs much faster than in DCM. Rapid bubbling is observed within 30 seconds in ACN while in DCM there is a few-minute induction period. Reactions in DCM lead to gel-like materials, whereas ACN gives a variety of precipitation products. This includes a crystalline product remaining at the bottom as well as foam products. The crystals are presumed to be polymeric since they are not soluble in THF (tetrahydrofuran) or DMF (dimethylformamide) which dissolve $Q_8M_8^H$.

Reactions conducted in acetone and methanol led to rapid gas release, but gels and/or precipitates were not observed until solvent removed, likely due to potential reactivity of the F^- activated Q-cage with the solvent as competing pathways.[17,23] Reactions in toluene led to gel formation directly, while mixed solvent 1:1 DCM:ACN gave a system containing gels and foams.

In our R-alkoxysilane work,[15,16] water content is an important reaction parameter. Therefore, water was added in both DCM and ACN model reactions to test its influence on reactivity. Due to immiscibility in DCM substantial influence was not found. Contrarily, ACN reactions were largely affected. After 5 min induction, gas evolution is rapid (**Fig. S1b**), resulting in foam-like products. Furthermore, the ACN+H_2O reactions lead to fine particulate products settled at the bottom of the reaction vessel as a side product.

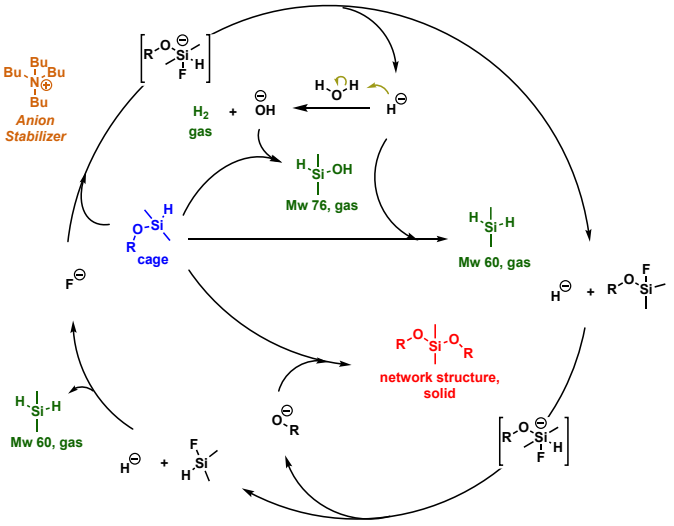

Scheme 2. Proposed fluoride ion catalyst pathways for the generation of porous polymers from $Q_8M_8^H$.

After ambient and vacuum drying, materials were characterized by scanning electron microscopy (SEM) to observe detailed structures and examined by powder X-ray diffraction (pXRD) to determine crystalline features. **Fig. 2a** shows materials from DCM reactions tend to dry out as amorphous glassy solids. Silica (SiO_2) itself is usually chemically inert to F^- salts, even with association.[24] Therefore, we expect that the cage itself would remain intact (**Fig. 3a**). However, pXRD results show that products from DCM reactions have no specific crystalline features and are amorphous (**Fig. 3b**). This suggests that either F^- ions in certain solvents destroy the silica core of $Q_8H_8^H$ or the polymerization process leaves cages intact to form highly complex 3-D polymers.

The products from ACN reactions were collected as two parts: the bottom crystalline product, and the gel from evaporated solvent. The crystalline product shows cubic structures in SEM images (**Fig. 2b**) and crystalline features in pXRD (**Fig. 3c**), similar in structure to those observed by Sato et al.,[8] suggesting connections between cages are ordered. Since gas evolved and the crystalline product has different solubility

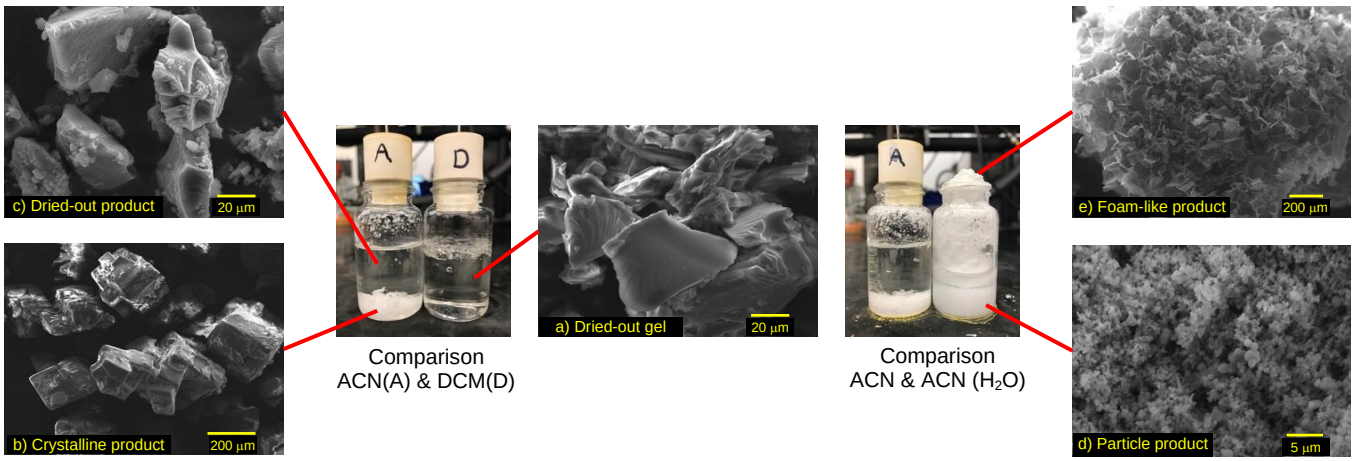

Fig. 2. SEM images of materials of a) dried out gel from DCM reaction. b) product from dried out ACN reaction solution. c) particles collected from bottom of ACN reaction. d) foam-like solid collected from the top of ACN reaction with 33mmol of additional water. e) polymer particles collected from the bottom of ACN reaction with 33 mmol of additional water.

than $Q_8H_8^H$ crystals (not soluble in DCM) reaction occurs. In ACN, F^- likely only attacks corner -$OSiMe_2H$ groups due to poorer $Q_8H_8^H$ solubility, and the reaction occurs with other nearby groups in a almost solid state reaction (**Scheme 1**).[8] The dried-out ACN reaction solution yielded similar featureless images as from the DCM gel product (**Fig. 2c**). Suggesting a less organized amorphous structure is formed through random cage linking with some periodicity observed in *p*XRD. With water, ACN reactions give two separate solid products: a particle product at the bottom and foam-like product from above the reaction flask. The particle product appears as small spheres with size of 1-3 mm by SEM (**Fig. 2d**) and shows crystalline structure in *p*XRD (**Fig. 3d**). Foam-like products show structures as layers of thin sheets clustered together (**Fig. 2d**) and no crystalline structure in *p*XRD. This suggests that the addition of water assists in increasing the reactivity of $Q_8H_8^H$ with very rapid gas evolution pushing the gelation product out as a foamed precipitate. The remaining particle products, which most likely stem form solid phase reactions result from similar methods to the crystalline products from ACN without water. These results show that this reaction has a wide versatility in forming a series of products depending on chosen conditions.

To explain the differences between these products, thermal gravimetric analysis (TGA), ^{29}Si MAS-NMR, FTIR, and surface area analysis (SSA) were carried out. For reactions in DCM, increasing water content caused a lowering of the ceramic yield (77.9% to 65.5%, **Fig. S4a**, in air) and SSA (26 m^2g^{-1} to 0 m^2g^{-1}, **Fig. S5a**), suggesting additional water increases propensity for non-cross-linked silanols. The fluctuation in TGA between 400-550 °C shows that water also increases the complexity of the structure. Release of trapped gas was observed when reaching the degradation temperature of the Si-O structure. IR spectra show no Si-H peaks at 2100 cm^{-1} suggesting that $SiMe_2H$ corners have been converted to other forms (**Fig. S6**). Si-C corresponding to Si-Me_2 groups[25] at 1260 cm^{-1} and a relatively narrow Si-O peak at ~1050 cm^{-1} are observed in all samples suggesting cages remain intact and methyl groups remain. ^{29}Si MAS NMR (**Fig. S7**) shows bridged dimethylsiloxane (D_2) peaks at -20 ppm, Q_3 at -101 ppm and Q_4 at -111 ppm corroborating both FTIR data and the proposed mechanism.[26,27] Pore size distributions show pores <50 Å, and water has low influence porosity (**Fig. S8**).

In ACN the crystalline product has an 81.8% CY (**Fig. 2b, S4b**), and a low SSA (59 m^2g^{-1} **Fig. S5a**), suggesting similarities to $Q_8M_8^H$, but with a slightly higher experimental CY (76.9%). Note expected CY for $Q_8M_8^H$ is 92.5% but corner loss complicates accuracy. Since the IR spectra show Si-H signal at 2100 cm^{-1} for the crystalline product, but not the dried-out product (**Fig. S9a**), the small increase in CY is likely caused by losing some $SiHMe_2OH$ or SiH_2Me_2 gas in the reaction. ^{29}Si MAS NMR (**Fig. S10**) shows narrow peaks like $Q_8M_8^H$,[28] but a broad and weak D_2 peak is evident (-20 ppm), suggesting some linkages between cages, leading to insolubility. Both Si-H and Si-OH groups are evident at -3.7 and -4.8 ppm respectively. Dried-out gel products show lower CY due to solvent trapping and or formed silanol groups. For these, pore size distribution shows crystalline products have mostly micropores (< 15Å), while the dried-out powder has pore sizes ~200 Å (**Fig. S12**). Low SSA (~60 m^2g^{-1}) for both are correlated with low pore volumes (~0.08 cm^2g^{-1}).

With water added (33.3 mmol), the $Q_8M_8^H$ crystals can be more effectively hydrolyzed/polymerized. This reaction yields both particles and foam-like products (**Fig. 2d, e**). Foam materials have higher CY (90%) compared to particle products (75%) (**Fig. S4b**), suggesting differences in reactivity. The IR spectra show that -$OSiMe_2H$ corners remain with Si-H signals at 2100 cm^{-1} (**Fig. S9b1**) in foams. This means bubbles pushed polymers out of the solution before they could fully condense. This is further confirmed with ^{29}Si MAS NMR (**Fig. S13**) which shows both cage-like (w/Si-H) and polymeric structures (D_2) simultaneously as well as incompletely condensed hydroxyls Q_3 (21% at -101 ppm) and D_1 (~<5%, 4.6 ppm). On the contrary, IR shows no Si-H signal at 2100 cm^{-1} for particle products (**Fig. S8b2**). This implies that $Q_8M_8^H$ crystals are fully broken down and condensed into new bridged structures (^{29}Si NMR **Fig. S14**). Both products have higher pore volumes (>0.15 cm^2g^{-1}) compared to original ACN reactions (0.08 cm^2g^{-1}) (**Fig. S12**), and therefore correspondingly higher SSA. Doubling the water to 66.6 mmol results in foams with lower accumulative pore volumes, leading to a decrease in SSA from 657 to 372 m^2g^{-1} and migration toward smaller pores.

Using other solvents such as acetone, methanol, toluene or 1:1 ACN:DCM result in similar products to those observed in the DCM and ACN systems discussed. No additional water was added to any of these solvent systems. By FTIR (**Fig. S15**) no Si-H groups remain for any of these solvents. Each showed mass loss below 200 °C in the TGA (**Fig. S16**), with toluene showing significant solvent trapping. All were amorphous with few structural features in *p*-XRD (**Fig. S17**). Porosity analysis (**Fig. S5** and **S18**) shows SSA values from 383 m^2g^{-1} (1:1 ACN:DCM) down to 107 m^2g^{-1} (methanol). Overall, clear correlations between the solvent polarity, reactivity, and properties were not obtained.[16]

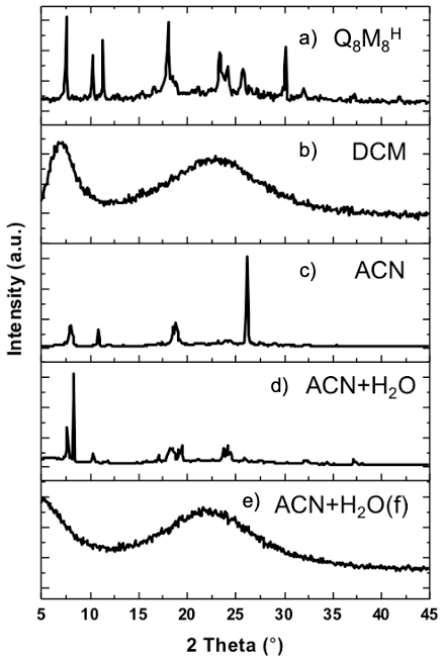

Fig. 3. *p*XRD Comparison for $Q_8H_8^H$ crystal and samples collected from reaction in different solvents. *(f) indicates foam-like product from corresponding reaction mixture.

Reactions with other catalysts CSF and TMAH were also somewhat effective to imbue network polymerization of $Q_8M_8^H$, see **SI** and **Figs. S4-S5**, **S9** and **S19-20** for details. Reactions with $Q_8M_8^{Me}$ showed no gas formation upon F^- addition and formed non-porous, non-network materials. See **Fig. S21-24** for characterization details. Future exploration will be undertaken into the properties of these materials and their potential uses.

In conclusion, our group developed a fast and efficient method to trigger self-polymerization of Q-type cages. Using $Q_8M_8^H$ as our model, we successfully observed a unique network polymerization using various solvents and found analogies to literature mechanisms. The Q-cages are primarily linked through D_2 groups as verified by FTIR and ^{29}Si NMR with seemingly little impact on Q-cage structure besides the peripheral groups. Depending on the solvent system and water content different types of networks can be formed including crystalline polymers (ACN), foams (ACN+H_2O), or a series of condensed gel materials in other solvents. All have porosities dependent on their synthetic parameters ranging from micro to mesoporous and SSA up to 657 m^2g^{-1}. These methods are useful in forming high silicon porous materials and nanostructured silica-rich crystals.

We thank Dan Conroy of Ohio State University for SSNMR experiments. This work supported in part by the U.S. National Science Foundation, Division of Materials Research through the LEAPS program #2137672.

References

1 S. D. Kimmins and N. R. Cameron, *Adv. Funct. Mater.*, 2011, **21**, 211–225.
2 S. Kitagawa, R. Kitaura and S. I. Noro, *Angew. Chemie - Int. Ed.*, 2004, **43**, 2334–2375.
3 M. Soldatov and H. Liu, *Prog. Polym. Sci.*, 2021, **119**, 101419.
4 W. Chaikittisilp, M. Kubo, T. Moteki, A. Sugawara-Narutaki, A. Shimojima and T. Okubo, *J. Am. Chem. Soc.*, 2011, **133**, 13832–13835.
5 Y. Kim, K. Koh, M. F. Roll, R. M. Laine and A. J. Matzger, *Macromolecules*, 2010, **43**, 6995–7000.
6 J. C. Furgal, H. Yamane, T. R. Odykirk, E. Yi, Y. Chujo and R. M. Laine, *Chem. - A Eur. J.*, 2018, **24**, 274–280.
7 A. Shimojima and K. Kuroda, *Molecules*, 2020, **25**, 1–11.
8 N. Sato, Y. Kuroda, H. Wada, A. Shimojima and K. Kuroda, *Chem. - A Eur. J.*, 2018, **24**, 17033–17038.
9 D. Pan, E. Yi, P. H. Doan, J. C. Furgal, M. Schwartz, S. Clark, T. Goodson III and R. M. Laine, *J. Ceram. Soc. Japan*, 2015, **123**, 756–763.
10 R. M. Laine, *J. Mater. Chem.*, 2005, **15**, 3725.
11 C. Zhang and R. M. Laine, *J. Am. Chem. Soc.*, 2000, **122**, 6979–6988.
12 N. Hu and J. C. Furgal, *Adv. Funct. Mater.*, 2021, **31**, 2010114.
13 A. Lusterio, M. Melendez-Zamudio and M. A. Brook, *Ind. Eng. Chem. Res.*, 2021, **60**, 3830–3838.
14 C. Zhang, F. Babonneau, C. Bonhomme, R. M. Laine, C. L. Soles, H. A. Hristov and A. F. Yee, *J. Am. Chem. Soc.*, 1998, **120**, 8380–8391.
15 N.-H. Hu and J. C. Furgal, *Materials (Basel).*, 2020, **13**, 1849.
16 N. H. Hu, C. U. Lenora, T. A. May, N. C. Hershberger and J. C. Furgal, *Mater. Chem. Front.*, 2020, **4**, 851–861.
17 K. Kuciński, H. Stachowiak-Dłużyńska and G. Hreczycho, *Coord. Chem. Rev.*, 2022, **459**, 214456.
18 D. Even and C. Berkland, *Int. J. Chem. Kinet.*, 2022, **54**, 478–487.
19 E. D. Voronova, I. E. Golub, A. Pavlov, N. V. Belkova, O. A. Filippov, L. M. Epstein and E. S. Shubina, *Inorg. Chem.*, 2020, **59**, 12240–12251.
20 I. S. Akhrem and M. Dene, *Bull. Acad. Sci. USSR Div. Chem. Sci.*, 1973, **22**, 897–899.
21 Y. El Aziz, A. R. Bassindale, P. G. Taylor, P. N. Horton, R. a. Stephenson and M. B. Hursthouse, *Organometallics*, 2012, **31**, 6032–6040.
22 S. Chanmungkalakul, V. Ervithayasuporn, S. Hanprasit, M. Masik, N. Prigyai and S. Kiatkamjornwong, *Chem. Commun.*, 2017, **53**, 12108–12111.
23 D. J. Parks and W. E. Piers, *J. Am. Chem. Soc.*, 1996, **118**, 9440–9441.
24 R. C. Specht, *Anal. Chem.*, 1956, **28**, 1015–1017.
25 D. R. Anderson, *Analysis of Silicones*, Wiley-Interscience, New York, 1974.
26 C. Corminbœuf, T. Heine and J. Weber, *Chem. Phys. Lett.*, 2002, **357**, 1–7.
27 F. Uhlig and H. C. Marsmann, *Si NMR Some Practical Aspects*, .
28 A. Sellinger and R. M. Laine, *Chem. Mater.*, 1996, **8**, 1592–1593.